

# Coupling Finite Elements and Auxiliary Sources

D. Casati and R. Hiptmair

Research Report No. 2018-04

February 2018

Latest revision: October 2019

Seminar für Angewandte Mathematik  
Eidgenössische Technische Hochschule  
CH-8092 Zürich  
Switzerland

# Coupling Finite Elements and Auxiliary Sources

D. Casati<sup>a,\*</sup>, R. Hiptmair<sup>a</sup>

<sup>a</sup>*ETH Zurich, Seminar for Applied Mathematics, Rämistrasse 101, 8092 Zurich,  
Switzerland*

---

## Abstract

We consider second-order scalar elliptic boundary value problems on unbounded domains, which model, for instance, electrostatic fields. We propose a discretization that relies on a Trefftz approximation by multipole auxiliary sources in some parts of the domain and on standard mesh-based primal Lagrangian finite elements in other parts. Several approaches are developed and, based on variational saddle point theory, rigorously analyzed to couple both discretizations across the common interface:

1. Least-squares-based coupling using techniques from PDE-constrained optimization.
2. Coupling through Dirichlet-to-Neumann operators.
3. Three-field variational formulation in the spirit of mortar finite element methods.

We compare these approaches in a series of numerical experiments.

*Keywords:* Finite Element Method, Multiple Multipole Program, Method of Auxiliary Sources, Trefftz method, computational electromagnetics

*2010 MSC:* 35Q61, 65N30, 65N80, 65Z05

---

\*Corresponding author

*Email addresses:* [daniele.casati@sam.math.ethz.ch](mailto:daniele.casati@sam.math.ethz.ch) (D. Casati),  
[hiptmair@sam.math.ethz.ch](mailto:hiptmair@sam.math.ethz.ch) (R. Hiptmair)

## 1. Introduction

As model problem we consider the second-order scalar elliptic transmission problem

$$\begin{aligned}
 -\nabla \cdot [\mathbf{A}(\mathbf{x}) \nabla u] &= f \quad \text{in } \mathbb{R}^d, \quad d = 2, 3, & (1a) \\
 u(\mathbf{x}) &= \begin{cases} c \log \|\mathbf{x}\| + \mathcal{O}(\|\mathbf{x}\|^{-1}) & \text{in } \mathbb{R}^2, \quad c \in \mathbb{R}, \\ \mathcal{O}(\|\mathbf{x}\|^{-1}) & \text{in } \mathbb{R}^3 \end{cases} \quad \text{for } \|\mathbf{x}\| \rightarrow \infty \text{ uniformly,} & (1b)
 \end{aligned}$$

where  $\mathbf{A} : \mathbb{R}^d \rightarrow \mathbb{R}^{d,d}$  is a symmetric, bounded, uniformly positive-definite diffusion coefficient. We assume that  $\mathbf{A}$  agrees with the identity matrix  $\mathbf{I} \in \mathbb{R}^{d,d}$  outside of a bounded domain  $\Omega_\star \subset \mathbb{R}^d$ :  $\mathbf{A}(\mathbf{x}) = \mathbf{I}$  for all  $\mathbf{x} \in \mathbb{R}^d \setminus \Omega_\star$ . In addition,  $f : \mathbb{R}^d \rightarrow \mathbb{R}$  has compact support in  $\Omega_\star$ . For the decay conditions (1b), please refer to [1, p. 259, Theorem 8.9].

Thus, the weak solution  $u \in H_{\text{loc}}^1(\mathbb{R}^d)$  of (1) is harmonic in  $\mathbb{R}^d \setminus \Omega_\star$ , i.e. it belongs to the continuous Trefftz space

$$\mathcal{T}(\mathcal{D}) := \left\{ v \in H_{\text{loc}}^1(\mathcal{D}) : \Delta v = 0, \right. \\
 \left. v \text{ satisfies decay conditions (1b)} \right\} \quad (2)$$

for  $\mathcal{D} = \mathbb{R}^d \setminus \Omega_\star$ .

Trefftz methods seek to approximate  $u$  on subdomains of  $\mathbb{R}^d \setminus \Omega_\star$  by means of some finite-dimensional subspace of  $\mathcal{T}(\mathcal{D})$ . Our method uses spaces spanned by potentials due to external multipole sources. We refer to them as the MMP approximation after the Trefftz method known as *Multiple Multipole Program*; see section 2 for details.

However, functions in a Trefftz space cannot approximate  $u$  in  $\Omega_\star$ . There we use a standard finite element space  $V_n$ ,  $V_n|_{\Omega_\star} \subset H^1(\Omega_\star)$ , together with the usual primal variational formulation of (1).

The two linked main issues arising are (i) the principle governing the selection of the MMP approximant and (ii) the coupling between the MMP domain and the Finite Element domain. Several options for (ii) will be proposed and discussed in section 3.

---

<sup>0</sup>*Abbreviations.* FEM: Finite Element Method. MMP: Multiple Multipole Program. Index **f** in formulas: FEM. Index **m** in formulas: MMP. MAS: Method of Auxiliary Sources. PDE: Partial Differential Equation. DtN: Dirichlet-to-Neumann.

### 1.1. Related Work

Trefftz methods for elliptic boundary value problems have a venerable history. A particular class are *Methods of Auxiliary Sources*, of which MMP is an example; see [2, 3] for comprehensive surveys.

Algorithm development of MAS has been pursued by groups worldwide, for instance in Georgia (group of R. Zaridse), UK [4], Greece [5, 6], Japan [7, 8, 9], Russia [10], and also at ETH Zurich (see section 2). Most simulations reported in the literature tackle dimensionally reduced 2D models (translational or rotational symmetry, Poisson’s or Helmholtz equation), but full 3D computations are becoming more common.

MAS coefficients are generally computed by least-squares or weighted residual methods, which simply enforce (weak) continuity and boundary conditions irrespectively of the considered PDE. On the other hand, Discontinuous Galerkin formulations for Trefftz methods arrive at a local variational formulation by applying integration by parts to the PDE, similarly to FEM. Together with A. Moiola and I. Perugia, the second author established a complete and rigorous convergence theory for the class of Discontinuous Galerkin Trefftz methods for both acoustic and electromagnetic scattering [11, 12, 13, 14, 15].

Concerning accuracy, it is universally reported that MAS achieves exponential convergence, provided that 1. the solution is smooth and possesses an analytic extension, and 2. both the curve  $\Sigma$  where the Trefftz functions are disposed and (adaptive) quadrature rules are chosen judiciously (see section 2.2 and [16, 17, 9]). However, in case of nonanalytic boundaries  $\Gamma$  of the MAS domain or nonsmooth data, it may not be possible to find an analytic extension of the solution beyond  $\Gamma$  at all. In 2D, this can be remedied by including special corner singular functions in the representation formula, see [17], or by letting  $\Gamma$  jut towards the corner [5, Section 4].

The ill-conditioning resulting from MAS augmentation, though inevitable, remains manageable [16]. In fact, MAS linear systems are usually ill-conditioned, something that can drastically reduce the accuracy. However, there exists a numerical algorithm that allows to obtain errors close to machine precision for the Helmholtz equation by performing a suitable change of basis [18].

Yet, there is no rigorous mathematical guidance for finding suitable curves  $\Sigma$  in 3D, especially if  $\Gamma$  features corners. For simple and canonical geometries, good choices can be made based on heuristics and experience, but this severely limits the applicability of pure MAS in 3D.

At the same time, little work has been devoted to the investigation of methods combining MAS with conventional finite element methods. To the best of our knowledge, this coupling has only been tackled from an engineering perspective.

Recently, J. Smajic, Ch. Hafner, and collaborators have demonstrated a simple methodology for FEM–MMP coupling at the level of 2D nonlinear magnetostatic analysis in [19]. Coupling is done by ad-hoc point matching of field values, the Dirichlet data, on the interface between the FEM and MMP domains (*collocation method*), while the Neumann data enter through a boundary term of the variational formulation. The resulting overdetermined FEM–MMP system of equations is solved in the least-squares sense.

### 1.2. Novelty & Outline

The authors are not aware of any prior work discussing the coupling of FEM and MAS from the perspective of numerical analysis. The approaches we propose to realize the coupling are described here for the first time.

After section 2 on MMP, the specific MAS employed in our work, in section 3 we illustrate the coupling approaches with details on their well-posedness and numerical stability. Numerical experiments are included in section 4, followed by some conclusive remarks (section 5).

## 2. MMP Trefftz Spaces

The concept of the Multiple Multipole Program was proposed by Ch. Hafner in his dissertation [20] based on the much older work of G. Mie and I. N. Vekua [21, 22]. Essentially, the Mie-Vekua approach approximates the field in a 2D multiply-connected domain by a multipole expansion (see section 2.1) supplemented with some generalized harmonic polynomials (Bessel functions). Extending these ideas, MMP introduces more multipoles (multiple multipoles) than required according to Vekua’s theory [22].

### 2.1. Multipoles

Basis functions spanning the MMP Trefftz spaces (2) are the so-called *multipoles*, potentials spawned by (anisotropic) point sources. This is why MMP belongs to the class of Methods of Auxiliary Sources (section 1.1). Given (2), multipoles are exact solutions of the homogeneous PDE  $\Delta u = 0$  subject to the decay conditions (1b).

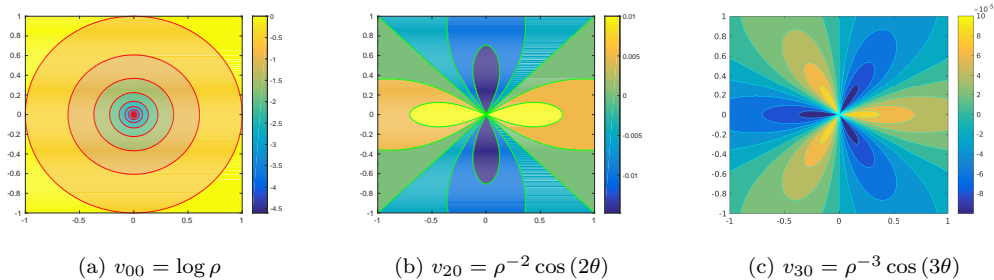


Figure 1: Sample multipoles of (3), i.e. basis functions of the 2D MMP Trefftz space (2).

A multipole can be written as  $v(\mathbf{x}) := f(r_{xc}) g(\theta_{xc})$  or  $v(\mathbf{x}) := f(r_{xc}) g(\theta_{xc}, \varphi_{xc})$  in a polar/spherical coordinate system in  $\mathbb{R}^2/\mathbb{R}^3$  ( $r \in [0, \infty)$ ,  $\theta \in [0, 2\pi)$ ,  $\varphi \in [0, \pi]$ ), with respect to its center  $\mathbf{c} \in \mathbb{R}^d$ ,  $d = 2, 3$ . Here,  $(r_{xc}, \theta_{xc}, \varphi_{xc})^\top$  are coordinates of the vector  $\mathbf{x}_c := \mathbf{x} - \mathbf{c}$ .

The function  $f(r_{xc})$  describing the radial dependence induces a singularity at the center  $\mathbf{c}$ , because  $|f(r)| \rightarrow \infty$  for  $r \rightarrow 0$ . It also yields the desired decay condition at infinity. Because of their singularity, multipoles must always be centered outside of the domain where they are used as a tool for approximation.

The spherical dependence  $g(\theta_{xc}, \varphi_{xc})$  is generally formulated in terms of spherical harmonics [1, p. 250]. The special multipoles chosen for our numerical experiments are:

$$\text{In } \mathbb{R}^2 : \quad \begin{cases} v_{00}(r_{xc}, \theta_{xc}) &= \log r_{xc} \\ v_{l0}(r_{xc}, \theta_{xc}) &= r_{xc}^{-l} \cos(l\theta_{xc}), \quad l = 1, \dots, \infty, \\ v_{l1}(r_{xc}, \theta_{xc}) &= r_{xc}^{-l} \sin(l\theta_{xc}), \quad l = 1, \dots, \infty. \end{cases} \quad (3)$$

Figure 1 shows three examples of multipoles according to (3) with center  $\mathbf{c} = \mathbf{0}$ .

$$\text{In } \mathbb{R}^3 : \quad v_{lm}(r_{xc}, \theta_{xc}, \varphi_{xc}) = r_{xc}^{-l-1} Y_{lm}(\theta_{xc}, \varphi_{xc}), \quad \begin{aligned} l &= 0, \dots, \infty \\ m &= -l, \dots, l \end{aligned} \quad (4)$$

Here,  $Y_{lm}(\theta, \varphi)$  are spherical harmonics [1, p. 250]. These multipoles are used for the numerical experiment of sections 4.1 and 4.2, and section 4.3. They also comply with (1b) [1, p. 259, Theorem 8.9].

Each multipole is characterized by a location, i.e. its center  $\mathbf{c}$ , and the (degree) parameters  $l$  and  $m$ . In our convergence studies we always place

several multipoles at a given location up to a certain order, which is the maximum degree of multipoles with that center. Hence, we use the term *multipole expansion* when referring to several multipoles in one point up to a certain order, which is the degree where the expansion is truncated. The total number of multipoles used for approximation is added to yield the total number of degrees of freedom of the discretization of the Trefftz space.

## 2.2. Approximation Properties

If the solution  $u$  of the 2-dimensional equation (1) possesses an analytic extension beyond the MMP domain  $\Omega_{\mathbf{m}} \in \mathbb{R}^2$ , into the region of  $\Omega_{\mathbf{m}}^c := \mathbb{R}^2 \setminus \Omega_{\mathbf{m}}$  between  $\Gamma := \partial\Omega_{\mathbf{m}}$  and the curve  $\Sigma$  along which the multipole expansions are placed, then we expect exponential convergence in terms of the number of degrees of freedom, both when the number of multipole expansions and the order of the expansions is raised. This result has been proven in [9, p. 1385, Theorem 4.1] for the dipole simulation method, but the author of [9] expects that the proof can be extended to MMP [9, p. 1392, Section 6].

Moreover, one can prove that convergence results in  $H^1$ -seminorm for harmonic polynomials inside a domain  $\Omega_{\star} \in \mathbb{R}^2$  also hold for multipoles in the complement  $\Omega_{\star}^c := \mathbb{R}^2 \setminus \Omega_{\star}$ . This is stated in the following theorem. A corresponding result for  $d = 3$  remains elusive.

**Proposition 1.** *Let  $d = 2$ . If the solution  $u: \Omega_{\star}^c \rightarrow \mathbb{R}$*

- *is harmonic in the complement  $\Omega_{\star}^c$  of a 2D bounded uniformly star-shaped [23, p. 56, Assumption 3.1.1] (w.r.t. the origin) domain  $\Omega_{\star}$ ,*
- *satisfies the decay condition (1b) at infinity,*
- *and possesses a harmonic extension into parts of the domain  $\Omega_{\star}$ ,*

*then its best approximation by multipoles located in the origin converges exponentially with respect to the order of the multipole expansion in the  $H^1$ -seminorm.*

*Proof.* The proof is based on the Kelvin transform [1, p. 259, Equation 8.30]:

$$u \rightarrow \Phi^* u \quad \text{with} \quad (\Phi^* u)(\mathbf{x}) := u(\Phi(\mathbf{x})), \quad \Phi(\mathbf{x}) := \frac{\mathbf{x}}{\|\mathbf{x}\|^2}, \quad \mathbf{x} \in \mathbb{R}^2 \setminus \{0\}. \quad (5)$$

For the  $H^1$ -seminorm we can show that

$$|u|_{H^1(\mathcal{D})} = |\Phi^* u|_{H^1(\Phi(\mathcal{D}))} \quad \forall u : \mathcal{D} \subset \mathbb{R}^2 \rightarrow \mathbb{R}, \quad (6)$$

where  $\mathcal{D}$  is any domain. When the Kelvin transform is applied to harmonic polynomials  $p(r, \theta) = r^l \text{cs}(l\theta)$ , with  $r, \theta$  polar coordinates,  $l \in \mathbb{Z}^*$ ,  $\text{cs} \in \{\cos, \sin\}$ , we obtain multipoles:

$$(\Phi^* p)(r, \theta) = r^{-l} \text{cs}(l\theta). \quad (7)$$

Let us now consider a solution  $u$  respecting the conditions stated above and the domain  $\Omega_{\mathbf{m}} := \Omega_{\star}^c$  where we want to estimate the MMP approximation. We first define  $\tilde{u} := u - c \log r$ ,  $c \in \mathbb{R}$ , whose decay condition is  $\tilde{u}(\mathbf{x}) = \mathcal{O}(\|\mathbf{x}\|^{-1})$  for  $\|\mathbf{x}\| \rightarrow \infty$  uniformly. Under the Kelvin transform,  $\Phi^* \tilde{u} = \mathcal{O}(\|\mathbf{x}\|)$  for  $\|\mathbf{x}\| \rightarrow 0$ .

Without loss of generality, we assume that  $\Phi(\Omega_{\mathbf{m}})$  contains the unit disk and  $\Phi^* \tilde{u}$  is harmonic in  $\Phi(\Omega_{\mathbf{m}})$ , which implies that  $\Phi^* \tilde{u}$  possesses a harmonic extension beyond  $\Phi(\Omega_{\mathbf{m}})$ . Thus we can conclude exponential convergence in  $H^1$ -seminorm for the approximation by harmonic polynomials of  $\Phi^* \tilde{u}$  in  $\Phi(\Omega_{\mathbf{m}})$  [23, p. 61, Remark 3.2.6]:

$$\begin{aligned} \forall p \in \mathbb{Z}^*, \quad \exists \alpha_l^{(p)}, \beta_l^{(p)} \in \mathbb{R}, \quad l = 1, \dots, p: \\ \left| \Phi^* \tilde{u} - \sum_{l=1}^p \alpha_l^{(p)} r^l \cos(l\theta) + \beta_l^{(p)} r^l \sin(l\theta) \right|_{H^1(\Phi(\Omega_{\mathbf{m}}))} \leq C q^p \quad (8a) \\ \text{for some } 0 \leq q \leq 1, \quad C \in \mathbb{R}^+ \text{ independent of } p. \end{aligned}$$

By applying (6) and (7) to (8a), we get that

$$\begin{aligned} \forall p \in \mathbb{Z}^*, \quad \exists \alpha_l^{(p)}, \beta_l^{(p)} \in \mathbb{R}, \quad l = 1, \dots, p: \\ \left| \tilde{u} - \sum_{l=1}^p \alpha_l^{(p)} r^{-l} \cos(l\theta) + \beta_l^{(p)} r^{-l} \sin(l\theta) \right|_{H^1(\Omega_{\mathbf{m}})} \leq C q^p \quad (8b) \\ \text{for some } 0 \leq q \leq 1, \quad C \in \mathbb{R}^+ \text{ independent of } p. \end{aligned}$$

Finally we can restore the proper decay condition of  $u$ ,  $u(\mathbf{x}) = c \log r + \mathcal{O}(\|\mathbf{x}\|^{-1})$  for  $\|\mathbf{x}\| \rightarrow \infty$ , where  $c \in \mathbb{R}$  is given by the coefficient  $\alpha_0^{(p)}$  of the zeroth-order multipole  $v_{00}(r, \theta) = \log r$  (see (3)). This concludes the proof.  $\square$

By means of a simple numerical experiment we illustrate these convergence results in  $\mathbb{R}^2$ .  $\Omega_{\mathbf{m}}$  is the complement of the unit square  $[0, 1]^2$ . We test the following solution which enjoys a  $\mathcal{O}(\|\mathbf{x}\|^{-1})$  decay for  $\|\mathbf{x}\| \rightarrow \infty$ :

$$u(\mathbf{x}) = \rho_{xc}^{-2} \sin(2\theta_{xc}), \quad (9)$$



where  $r_{xc} \in [0, \infty)$  and  $\theta_{xc} \in [0, 2\pi)$  are polar coordinates of vector  $\mathbf{x} - \mathbf{c}$ . We consider two positions of  $\mathbf{c}$ :  $(0.4, 0.4)^\top$  and  $(0.2, 0.2)^\top$ . (9) represents a harmonic function  $\in H^1(\mathbb{R}^2 \setminus [0, 1]^2)$  that uniformly decays for  $\|\mathbf{x}\| \rightarrow \infty$  with a singularity in  $\mathbf{c}$ .

Multipoles are chosen from (3). We consider two configurations:

1. Multipole expansions up to a fixed order 1 uniformly located on a circle at the center of the unit square  $[0, 1]^2$  with radius 0.25. During the test we increase the number of expansions.

Note that, given this choice of multipoles, the singularity of the solution with  $\mathbf{c} = (0.4, 0.4)^\top$  lies inside the circle of multipoles, i.e. the solution has an analytic extension between  $\Gamma$  and the circle of multipoles  $\Sigma$ . On the other hand, the solution with  $\mathbf{c} = (0.2, 0.2)^\top$  has the singularity outside  $\Sigma$  and does not have an analytic extension.

2. A single multipole expansion of a given order placed in the center of the unit square  $[0, 1]^2$ . During the test we increase the order.

We compute the best approximation of the solutions in spaces spanned by multipoles by means of the collocation method on uniformly spaced points on the edges of the unit square (corners are avoided). The number of points is chosen to make the overdetermined system almost square. The system is then solved by QR decomposition.

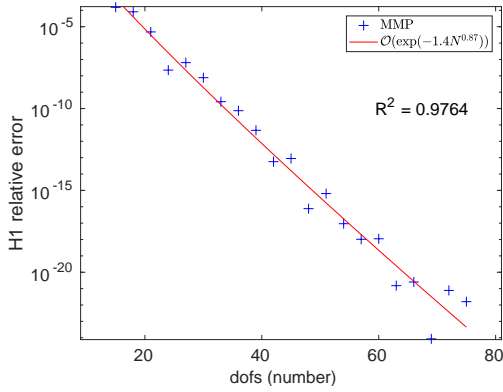
The approximation error in  $H^1$ -seminorm is computed using

$$\int_{\Omega_{\mathbf{m}}} |\nabla(u - u_{\mathbf{m}})|^2 d\mathbf{x} = \int_{\partial\Omega_{\mathbf{m}}} (u - u_{\mathbf{m}}) [\mathbf{n} \cdot \nabla(u - u_{\mathbf{m}})] dS \quad (10)$$

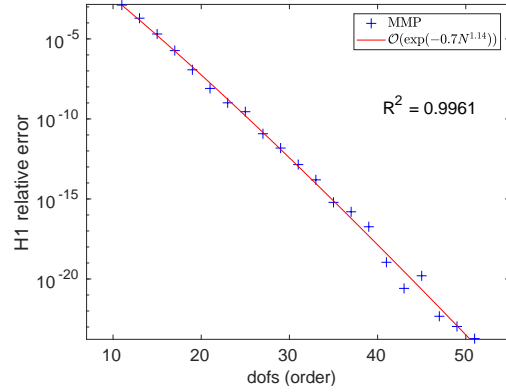
and the integral is approximated by Gaussian quadrature.

For the solution with an analytic extension ( $\mathbf{c} = (0.4, 0.4)^\top$ ), we observe exponential convergence given both fixed-order multipole expansions on a circle and one variable-order expansion placed in the origin, as shown in figs. 2a and 2b, respectively. This is in accordance with Proposition 1 and the literature.

For the solution without an analytic extension ( $\mathbf{c} = (0.2, 0.2)^\top$ ), we see convergence from fig. 3, but without the same regular pattern as fig. 2 (and the error is much higher).

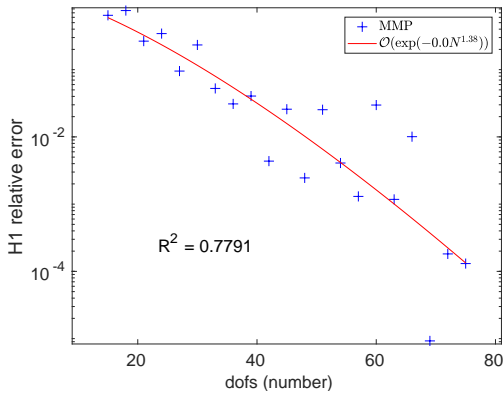


(a) Increasing number of expansions.

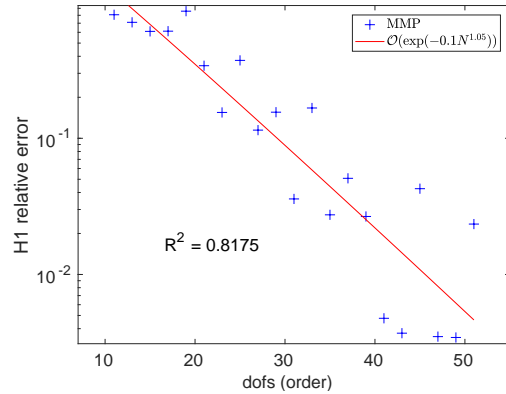


(b) Expansion with increasing order.

Figure 2: Convergence plots of MMP for solution  $\rho_{xc}^{-2} \sin(2\theta_{xc})$  with  $\mathbf{c} = (0.4, 0.4)^\top$ . The error-dimension is in logarithmic scale. The exponential convergence curve  $C \exp(-\gamma N^\delta)$ ,  $C, \gamma, \delta \in \mathbb{R}$ , is fitted to the data.



(a) Increasing number of expansions.



(b) Expansion with increasing order.

Figure 3: Convergence plots of MMP for solution  $\rho_{xc}^{-2} \sin(2\theta_{xc})$  with  $\mathbf{c} = (0.2, 0.2)^\top$ . The error-dimension is in logarithmic scale. The exponential convergence curve  $C \exp(-\gamma N^\delta)$ ,  $C, \gamma, \delta \in \mathbb{R}$ , is fitted to the data.

### 3. Coupling Strategies

We consider the partition  $\mathbb{R}^d = \Omega_f \cup \Gamma \cup \Omega_m$ ,  $d = 2, 3$ ,  $\Gamma := \partial\Omega_f = \partial\Omega_m$ ,  $\Omega_f \cap \Omega_m = \emptyset$ .  $\Omega_f$  is a bounded Lipschitz domain, the FE domain, whereas  $\Omega_m$  is dubbed the MMP domain. The terminology indicates the type of approximation of  $u$  to be employed in the subdomain. Coupling is done across the interface  $\Gamma$ . We demand  $\Omega_\star \subset \Omega_f$ , but not necessarily  $\Omega_\star = \Omega_f$ . If  $\Omega_\star \neq \Omega_f$ . In this case  $\Gamma$  is an *artificial interface*.

We define

$$u^f := u|_{\Omega_f} \in H^1(\Omega_f), \quad u^m := u|_{\Omega_m} \in H_{\text{loc}}^1(\Omega_m). \quad (11)$$

As natural norms we use *energy norms*. For  $u^f$  defined on the bounded domain  $\Omega_f$ , the energy norm is  $\|u^f\|_{H^1(\Omega_f)}$ . For  $u^m \in \mathcal{T}(\Omega_m)$  and  $d = 3$ , we use  $\|u^m\|_{\mathcal{T}(\Omega_m)} := |u^m|_{H^1(\Omega_m)} := \|\nabla u^m\|_{L^2(\Omega_m)}$ . For  $d = 2$ , the energy norm is not necessarily well-defined. In this case we rely on the norm

$$\|u^m\|_{\mathcal{T}(\Omega_m)} := |c| + \|\nabla(u^m - c \log\|\mathbf{x}\|)\|_{L^2(\Omega_m)}. \quad (12)$$

with  $c \in \mathbb{R}$ , such that

$$(u^m - c \log\|\mathbf{x}\|)(\mathbf{x}) = \mathcal{O}(\|\mathbf{x}\|^{-1}) \text{ for } \|\mathbf{x}\| \rightarrow \infty. \quad (13)$$

We denote by  $\gamma_{\mathbf{n}}$  the *co-normal trace operator*  $\gamma_{\mathbf{n}} : H_{\text{loc}}^1(\Delta, \Omega_\circ) \rightarrow H^{-\frac{1}{2}}(\Gamma)$ ,  $\gamma_{\mathbf{n}}v := \mathbf{n} \cdot \mathbf{A}\nabla v$ ,  $v \in H_{\text{loc}}^1(\Delta, \Omega_\circ)$ ,  $H_{\text{loc}}^1(\Delta, \Omega_\circ)$  the space of functions  $v \in H_{\text{loc}}^1(\Omega_\circ)$  for which  $\Delta v \in L_{\text{loc}}^2(\Omega_\circ)$ , given  $\circ = \mathbf{f}, \mathbf{m}$ . We always take  $\mathbf{n}$  as the normal pointing outwards with respect to  $\Omega_f$  into  $\Omega_m$ .

Across  $\Gamma$  the solution  $u$  of (1) has to satisfy the *transmission conditions* [24, p. 107, Lemma 5.3]

$$u^f|_{\Gamma} = u^m|_{\Gamma}, \quad (14a)$$

$$\gamma_{\mathbf{n}}u^f|_{\Gamma} = \gamma_{\mathbf{n}}u^m|_{\Gamma}. \quad (14b)$$

The starting point of all the coupling approaches is the weak form of (1) in  $\Omega_f$ . By testing the PDE with  $v^f \in H^1(\Omega_f)$ , integrating by parts over  $\Omega_f$ , and using the transmission condition (14b), we obtain

$$\int_{\Omega_f} \mathbf{A}\nabla u^f \cdot \nabla v^f \, d\mathbf{x} - \int_{\Gamma} \gamma_{\mathbf{n}}u^m v^f \, dS = \int_{\Omega_f} f v^f \, d\mathbf{x} \quad \forall v^f \in H^1(\Omega_f). \quad (15)$$

Depending on how we impose the additional transmission condition (14a), we end up with different coupling approaches that lead to different *linear variational saddle point problems* to be discussed in the following sections. Throughout, we will rely on the abstract saddle point theory, as presented, for instance, in [25, Chapter III, Section 4].

### 3.1. PDE-constrained Least-Squares Coupling

Taking the cue from (14a), we seek  $u^f \in H^1(\Omega_f)$ ,  $u^m \in \mathcal{T}(\Omega_m)$ ,

- minimizing

$$J_\Gamma(u^f, u^m) := \|u^f - u^m\|_{L^2(\Gamma)}^2 \quad (16)$$

- and satisfying the constraint (15).

This is a quadratic minimization problem under a linear variational constraint, whose necessary and sufficient optimality conditions (*KKT-conditions*) give rise to the following saddle point problem:

$$\begin{aligned} & \text{Seek } u^f \in H^1(\Omega_f), u^m \in \mathcal{T}(\Omega_m), p^f \in H^1(\Omega_f): \\ & \begin{cases} \mathfrak{a}^{\text{LS}}((u^f, u^m), (v^f, v^m)) + \mathfrak{b}^{\text{LS}}((v^f, v^m), p^f) = 0 \\ \mathfrak{b}^{\text{LS}}((u^f, u^m), q^f) = \int_{\Omega_f} f q^f \, d\mathbf{x} \end{cases} \\ & \forall v^f \in H^1(\Omega_f), \forall v^m \in \mathcal{T}(\Omega_m), \forall q^f \in H^1(\Omega_f), \end{aligned} \quad (17)$$

where

$$\mathfrak{a}^{\text{LS}}((u^f, u^m), (v^f, v^m)) := \int_{\Gamma} (u^f - u^m)(v^f - v^m) \, dS, \quad (18a)$$

$$\mathfrak{b}^{\text{LS}}((u^f, u^m), q^f) := \int_{\Omega_f} \mathbf{A} \nabla u^f \cdot \nabla q^f \, d\mathbf{x} - \int_{\Gamma} \gamma_{\mathbf{n}} u^m q^f \, dS. \quad (18b)$$

The constraint implied by the second line of (17) uniquely defines a function  $u^f = u^f(u^m)$ , satisfying  $\gamma_{\mathbf{n}} u^f = \gamma_{\mathbf{n}} u^m$  from (14b). Thus, the existence and uniqueness of a solution to (17) follows from those for (1). However, stability in energy norms cannot be expected as  $\mathfrak{a}^{\text{LS}}$  fails to be coercive on the kernel of  $\mathfrak{b}^{\text{LS}}$ .

**Remark 1.** If we relied on the  $H^{\frac{1}{2}}(\Gamma)$ -inner product  $\langle \cdot, \cdot \rangle_{H^{\frac{1}{2}}(\Gamma)}$  and defined

$$a^{\text{LS}}((u^{\text{f}}, u^{\text{m}}), (v^{\text{f}}, v^{\text{m}})) := \langle u^{\text{f}} - u^{\text{m}}, v^{\text{f}} - v^{\text{m}} \rangle_{H^{\frac{1}{2}}(\Gamma)}, \quad (19)$$

then the *ellipticity on the kernel* condition of abstract saddle point theory would be satisfied for (17). To see it note that, if  $(u^{\text{f}}, u^{\text{m}}) \in H^1(\Omega_{\text{f}}) \times \mathcal{T}(\Omega_{\text{m}})$  satisfy  $b^{\text{LS}}((u^{\text{f}}, u^{\text{m}}), q^{\text{f}}) = 0$  for all  $q^{\text{f}} \in H^1(\Omega_{\text{f}})$ , then integration by parts in  $\Omega_{\text{m}}$  shows

$$|u^{\text{f}}|_{H^1(\Omega_{\text{f}})}^2 + |u^{\text{m}}|_{H^1(\Omega_{\text{m}})}^2 \leq C \left\{ \|u^{\text{f}} - u^{\text{m}}\|_{H^{\frac{1}{2}}(\Gamma)}^2 + \|\gamma_{\text{n}} u^{\text{f}} - \gamma_{\text{n}} u^{\text{m}}\|_{H^{-\frac{1}{2}}(\Gamma)}^2 \right\} \quad (20)$$

for some  $C \in \mathbb{R}^+$ . The second term on the right-hand side vanishes. Yet, the  $H^{\frac{1}{2}}(\Gamma)$ -inner product is nonlocal and, consequently, not suitable for numerical purposes.

The Galerkin discretization of (17) is straightforward:

1. We replace  $H^1(\Omega_{\text{f}})$  with a Lagrangian finite element space<sup>1</sup>  $V_n$  built on a mesh of  $\Omega_{\text{f}}$ .
2. We approximate  $u^{\text{m}}$  and  $v^{\text{m}}$  in a finite-dimensional Trefftz space  $\mathcal{T}_n \subset \mathcal{T}(\Omega_{\text{m}})$ .

We appeal to variational saddle point theory and note that a uniform discrete *inf-sup condition* of abstract saddle point theory for  $b^{\text{LS}}$  is immediate.

Yet, ellipticity on the discrete kernel,

$$\ker_n b^{\text{LS}} := \{(v_n^{\text{f}}, v_n^{\text{m}}) \in V_n \times \mathcal{T}_n : b^{\text{LS}}((v_n^{\text{f}}, v_n^{\text{m}}), q^{\text{f}}) = 0 \quad \forall q^{\text{f}} \in V_n\}, \quad (21)$$

hinges on an inverse inequality. Define

$$K_n := \sup \left\{ \|\gamma_{\text{n}} u_n^{\text{m}}\|_{L^2(\Gamma)} : u_n^{\text{m}} \in \mathcal{T}_n, \|\gamma_{\text{n}} u_n^{\text{m}}\|_{H^{-\frac{1}{2}}(\Gamma)} = 1 \right\}. \quad (22)$$

By the equivalence of all norms on finite dimensional spaces, a finite  $K_n \in \mathbb{R}^+$  will exist. Let  $(u_n^{\text{f}}, u_n^{\text{m}}) \in \ker_n b^{\text{LS}}$ . This means that  $\int_{\Gamma} \gamma_{\text{n}} u_n^{\text{m}} \, dS = 0$ , which

---

<sup>1</sup>The subscript  $n$  tags spaces, functions, etc. connected with *discrete* transmission problems.

implies  $\nabla u_n^{\mathbf{m}}(\mathbf{x}) = \mathcal{O}(\|\mathbf{x}\|^{-2})$ . As a consequence,  $\nabla u_n^{\mathbf{m}} \in L^2(\Omega_{\mathbf{m}})$  also for  $d = 2$ . Thus, we get

$$\int_{\Omega_{\mathbf{f}}} \mathbf{A} \nabla u_n^{\mathbf{f}} \cdot \nabla u_n^{\mathbf{f}} \, d\mathbf{x} + \int_{\Omega_{\mathbf{m}}} \|\nabla u_n^{\mathbf{m}}\|^2 \, d\mathbf{x} = \int_{\Gamma} (u_n^{\mathbf{f}} - u_n^{\mathbf{m}}) \gamma_{\mathbf{n}} u_n^{\mathbf{m}} \, dS. \quad (23)$$

We conclude that, with  $C \in \mathbb{R}^+$  independent of the choice of both  $V_n$  and  $\mathcal{T}_n$ ,

$$\|\nabla u_n^{\mathbf{f}}\|_{L^2(\Omega_{\mathbf{f}})}^2 + \|\nabla u_n^{\mathbf{m}}\|_{L^2(\Omega_{\mathbf{m}})}^2 \leq C \|u_n^{\mathbf{f}} - u_n^{\mathbf{m}}\|_{L^2(\Gamma)} \cdot \|\gamma_{\mathbf{n}} u_n^{\mathbf{m}}\|_{L^2(\Gamma)}. \quad (24)$$

Next, we use the inverse inequality implicit in (22) together with the estimate  $\|\gamma_{\mathbf{n}} u^{\mathbf{m}}\|_{H^{-\frac{1}{2}}(\Gamma)} \leq C \|\nabla u^{\mathbf{m}}\|_{L^2(\Omega_{\mathbf{m}})} \quad \forall u^{\mathbf{m}} \in \mathcal{T}(\Omega_{\mathbf{m}})$ ,  $C \in \mathbb{R}^+$ , and obtain

$$\|\nabla u_n^{\mathbf{f}}\|_{L^2(\Omega_{\mathbf{f}})} + \|\nabla u_n^{\mathbf{m}}\|_{L^2(\Omega_{\mathbf{m}})} \leq C K_n \|u_n^{\mathbf{f}} - u_n^{\mathbf{m}}\|_{L^2(\Gamma)}, \quad (25)$$

which proves the ellipticity of  $\mathbf{a}^{\text{LS}}$  on  $\ker_n \mathbf{b}^{\text{LS}}$ , albeit with a constant  $K_n$  tending to zero as the Trefftz space  $\mathcal{T}_n$  is refined. Hence, the discrete variational problem is stable, but convergence is guaranteed only if, asymptotically, the approximation errors decay faster than  $K_n$  increases.

### 3.2. Dirichlet-to-Neumann-based Coupling

We take into account the continuity transmission condition (14a) in weak form, testing it with co-normal traces  $\gamma_{\mathbf{n}} v^{\mathbf{m}}$  of  $v^{\mathbf{m}} \in \mathcal{T}(\Omega_{\mathbf{m}})$ :

$$\int_{\Gamma} u^{\mathbf{f}} \gamma_{\mathbf{n}} v^{\mathbf{m}} \, dS - \int_{\Gamma} u^{\mathbf{m}} \gamma_{\mathbf{n}} v^{\mathbf{m}} \, dS = 0 \quad \forall v^{\mathbf{m}} \in \mathcal{T}(\Omega_{\mathbf{m}}). \quad (26)$$

Combining (26) with the variational form of (15), we end up with:

Seek  $u^{\mathbf{f}} \in H^1(\Omega_{\mathbf{f}})$ ,  $u^{\mathbf{m}} \in \mathcal{T}(\Omega_{\mathbf{m}})$ :

$$\begin{cases} \int_{\Omega_{\mathbf{f}}} \mathbf{A} \nabla u^{\mathbf{f}} \cdot \nabla v^{\mathbf{f}} \, d\mathbf{x} - \int_{\Gamma} \gamma_{\mathbf{n}} u^{\mathbf{m}} v^{\mathbf{f}} \, dS = \int_{\Omega_{\mathbf{f}}} f v^{\mathbf{f}} \, d\mathbf{x} & \forall v^{\mathbf{f}} \in H^1(\Omega_{\mathbf{f}}) \\ \int_{\Gamma} u^{\mathbf{f}} \gamma_{\mathbf{n}} v^{\mathbf{m}} \, dS - \int_{\Gamma} u^{\mathbf{m}} \gamma_{\mathbf{n}} v^{\mathbf{m}} \, dS = 0 & \forall v^{\mathbf{m}} \in \mathcal{T}(\Omega_{\mathbf{m}}) \end{cases} \quad (27)$$

The analysis of (27) on both the continuous and discrete levels is based on splitting  $u^{\mathbf{f}}, v^{\mathbf{f}} \in H^1(\Omega_{\mathbf{f}})$  as

$$\begin{aligned} u^{\mathbf{f}} &= u_{\star}^{\mathbf{f}} + \mu, & u_{\star}^{\mathbf{f}}, v_{\star}^{\mathbf{f}} &\in H_{\star}^1(\Omega_{\mathbf{f}}) := \left\{ w \in H^1(\Omega_{\mathbf{f}}) : \int_{\Omega_{\mathbf{f}}} w \, d\mathbf{x} = 0 \right\}, \mu, \nu \in \mathbb{R}, \\ v^{\mathbf{f}} &= v_{\star}^{\mathbf{f}} + \nu, \end{aligned} \quad (28)$$

which leads to the following saddle point problem:

Seek  $u_\star^f \in H_\star^1(\Omega_f)$ ,  $u^m \in \mathcal{T}(\Omega_m)$ ,  $\mu \in \mathbb{R}$ :

$$\begin{cases} \int_{\Omega_f} \mathbf{A} \nabla u_\star^f \cdot \nabla v_\star^f \, d\mathbf{x} - \int_{\Gamma} \gamma_n u^m v_\star^f \, dS & = \int_{\Omega_f} f v_\star^f \, d\mathbf{x} \\ \int_{\Gamma} u_\star^f \gamma_n v^m \, dS - \int_{\Gamma} u^m \gamma_n v^m \, dS + \int_{\Gamma} \mu \gamma_n v^m \, dS & = 0 \\ - \int_{\Gamma} \gamma_n u^m \, dS & = \int_{\Omega_f} f \, d\mathbf{x} \end{cases} \quad (29)$$

$\forall v_\star^f \in H_\star^1(\Omega_f)$ ,  $\forall v^m \in \mathcal{T}(\Omega_m)$ .

Galerkin discretization of (29) is straightforward: as in section 3.1, we replace  $H^1(\Omega_f)$  with a Lagrangian finite element space and  $\mathcal{T}(\Omega_m)$  with a finite-dimensional subspace  $\mathcal{T}_n$ .

To apply saddle point theory to (29), let us define the following operators:

$$\begin{aligned} \mathbf{a}^{\text{DtN}}((u_\star^f, u^m), (v_\star^f, v^m)) &:= \int_{\Omega_f} \mathbf{A} \nabla u_\star^f \cdot \nabla v_\star^f \, d\mathbf{x} - \int_{\Gamma} \gamma_n u^m v_\star^f \, dS + \\ &+ \int_{\Gamma} u_\star^f \gamma_n v^m \, dS - \int_{\Gamma} u^m \gamma_n v^m \, dS, \end{aligned} \quad (30a)$$

$$\mathbf{b}^{\text{DtN}}(u^m, \mu) := \int_{\Gamma} \gamma_n u^m \mu \, dS. \quad (30b)$$

For  $u^m \in \ker \mathbf{b}^{\text{DtN}}$ , we have that  $\int_{\Gamma} \gamma_n u^m \, dS = 0$ , which implies  $\nabla u^m(\mathbf{x}) = \mathcal{O}(\|\mathbf{x}\|^{-2})$  for  $\|\mathbf{x}\| \rightarrow \infty$ . As a consequence,

$$\mathbf{a}^{\text{DtN}}((u_\star^f, u^m), (u_\star^f, u^m)) = \int_{\Omega_f} \mathbf{A} \nabla u_\star^f \cdot \nabla u_\star^f \, d\mathbf{x} + \int_{\Omega_m} \|\nabla u^m\|^2 \, d\mathbf{x}. \quad (31)$$

This proves the ellipticity on the kernel in both the continuous and discrete settings: the variational problems are uniformly stable. The inf-sup condition for  $\mathbf{b}^{\text{DtN}}$  of (30b) is trivial considering that  $\mu \in \mathbb{R}$  and  $\int_{\Gamma} \gamma_n u^m \, dS \neq 0$  for some  $u^m \in \mathcal{T}(\Omega_m)$ .

### 3.3. Multi-Field Coupling

We introduce the unknown  $\lambda := \gamma_n u^m$  and insert it into (15), while we enforce both the defining equation  $\lambda := \gamma_n u^m$  and the transmission condition

(14a) in a weak sense. Note that (14a) is an equation connecting traces in  $H^{\frac{1}{2}}(\Gamma)$  and therefore it has to be tested with functions in the dual space  $H^{-\frac{1}{2}}(\Gamma)$ . We end up with:

$$\begin{aligned} & \text{Seek } u^{\mathbf{f}} \in H^1(\Omega_{\mathbf{f}}), u^{\mathbf{m}} \in \mathcal{T}(\Omega_{\mathbf{m}}), \lambda \in H^{-\frac{1}{2}}(\Gamma): \\ & \begin{cases} \int_{\Omega_{\mathbf{f}}} \mathbf{A} \nabla u^{\mathbf{f}} \cdot \nabla v^{\mathbf{f}} \, d\mathbf{x} & - \int_{\Gamma} \lambda v^{\mathbf{f}} \, dS & = \int_{\Omega_{\mathbf{f}}} f v^{\mathbf{f}} \, d\mathbf{x} \\ & - \int_{\Gamma} \gamma_{\mathbf{n}} u^{\mathbf{m}} v^{\mathbf{m}} \, dS + \int_{\Gamma} \lambda v^{\mathbf{m}} \, dS & = 0 \\ - \int_{\Gamma} u^{\mathbf{f}} v_{\lambda} \, dS + \int_{\Gamma} u^{\mathbf{m}} v_{\lambda} \, dS & & = 0 \end{cases} \\ & \forall v^{\mathbf{f}} \in H^1(\Omega_{\mathbf{f}}), \forall v^{\mathbf{m}} \in \mathcal{T}(\Omega_{\mathbf{m}}), \forall v_{\lambda} \in H^{-\frac{1}{2}}(\Gamma). \end{aligned} \quad (32)$$

For the Galerkin discretization of (32), we replace  $H^1(\Omega_{\mathbf{f}})$  with a Lagrangian finite element space  $V_n$  and  $\mathcal{T}(\Omega_{\mathbf{m}})$  with a finite-dimensional subspace  $\mathcal{T}_n$ , as in sections 3.1 and 3.2. For discretizing  $\lambda$  we use the traces of the finite element functions in  $V_n$  on the boundary.

In order to apply saddle point theory to (32), let us consider the left-hand side of (32) and define the following bilinear form:

$$a^{\text{MF}}((u^{\mathbf{f}}, u^{\mathbf{m}}), (v^{\mathbf{f}}, v^{\mathbf{m}})) := \int_{\Omega_{\mathbf{f}}} \mathbf{A} \nabla u^{\mathbf{f}} \cdot \nabla v^{\mathbf{f}} \, d\mathbf{x} - \int_{\Gamma} \gamma_{\mathbf{n}} u^{\mathbf{m}} v^{\mathbf{m}} \, dS. \quad (33)$$

Let us also define

$$b^{\text{MF}}((u^{\mathbf{f}}, u^{\mathbf{m}}), \lambda) := \int_{\Gamma} (u^{\mathbf{f}} - u^{\mathbf{m}}) \lambda \, dS. \quad (34)$$

We restrict ourselves to  $d = 3$  and observe that, in this case,

$$a^{\text{MF}}((u^{\mathbf{f}}, u^{\mathbf{m}}), (u^{\mathbf{f}}, u^{\mathbf{m}})) = \int_{\Omega_{\mathbf{f}}} \mathbf{A} \nabla u^{\mathbf{f}} \cdot \nabla u^{\mathbf{f}} \, d\mathbf{x} + \int_{\Omega_{\mathbf{m}}} \|\nabla u^{\mathbf{m}}\|^2 \, d\mathbf{x}. \quad (35)$$

In the continuous case we have that

$$\ker b^{\text{MF}} = \{v^{\mathbf{f}} \in H^1(\Omega_{\mathbf{f}}), v^{\mathbf{m}} \in \mathcal{T}(\Omega_{\mathbf{m}}) : v^{\mathbf{f}} = v^{\mathbf{m}} \text{ on } \Gamma\} \quad (36)$$

and ellipticity on the kernel is clear because  $a^{\text{MF}}$  induces a norm on  $\ker b^{\text{MF}}$  that is equivalent to the energy norm.



In the discrete case, since  $V_n$  contains constant functions, the kernel of  $\mathbf{a}^{\text{MF}}$  again contains only piecewise constant functions inside  $\Omega_{\mathbf{f}}$  combined with the zero function in  $\Omega_{\mathbf{m}}$ . Obviously, the intersection of this space with the discrete kernel  $\ker_n \mathbf{b}^{\text{MF}}$  must be trivial. This amounts to ellipticity on the kernel in the discrete case.

The continuous inf-sup condition for  $\mathbf{b}^{\text{MF}}$  is a consequence of the duality of  $H^{\frac{1}{2}}(\Gamma)$  and  $H^{-\frac{1}{2}}(\Gamma)$ .

We discuss the discrete inf-sup condition for the concrete case of piecewise linear Lagrangian finite elements on a tetrahedral mesh  $\mathcal{M}_{\mathbf{f}}$  of  $\Omega_{\mathbf{f}}$ :  $V_n = \mathcal{S}_1^0(\mathcal{M}_{\mathbf{f}})$ , with

$$\begin{aligned} \mathcal{S}_1^0(\mathcal{M}_{\mathbf{f}}) := \{ & v \in C^0(\Omega_{\mathbf{f}}) : \forall K \in \mathcal{M}_{\mathbf{f}} : v|_K(\mathbf{x}) = \alpha_K + \boldsymbol{\beta}_K \cdot \mathbf{x}, \\ & \alpha_K \in \mathbb{R}, \boldsymbol{\beta}_K \in \mathbb{R}^3, \mathbf{x} \in K\} \subset H^1(\Omega_{\mathbf{f}}), \quad \mathcal{M}_{\mathbf{f}} \text{ mesh of } \Omega_{\mathbf{f}}. \end{aligned} \quad (37)$$

The  $H^{-\frac{1}{2}}$ -norm of  $\lambda_n \in V_n$  can be expressed as

$$\|\lambda_n\|_{H^{-\frac{1}{2}}(\Gamma)} := \sup_{v \in H^{\frac{1}{2}}(\Gamma)} \frac{\int_{\Gamma} \mathbf{Q}_n v \lambda_n \, dS}{\|v\|_{H^{\frac{1}{2}}(\Gamma)}} \leq C \sup_{v \in H^{\frac{1}{2}}(\Gamma)} \frac{\int_{\Gamma} \mathbf{Q}_n v \lambda_n \, dS}{\|\mathbf{Q}_n v\|_{H^{\frac{1}{2}}(\Gamma)}}, \quad (38)$$

where  $\mathbf{Q}_n : L^2(\Gamma) \rightarrow V_n|_{\Gamma}$  is the  $L^2$ -orthogonal projection operator such that, given  $u \in L^2(\Gamma)$ ,

$$\mathbf{Q}_n u \in V_n|_{\Gamma} : \int_{\Gamma} (u - \mathbf{Q}_n u) v_n \, dS = 0 \quad \forall v_n \in V_n. \quad (39)$$

Under mild assumptions on the surface mesh  $\mathcal{M}_{\mathbf{f}}|_{\Gamma}$ , we have that  $\|\mathbf{Q}_n u_{\Gamma}\|_{H^1(\Gamma)} \leq C \|u_{\Gamma}\|_{H^1(\Gamma)} \quad \forall u_{\Gamma} \in H^1(\Gamma)$ ,  $C \in \mathbb{R}^+$  independent of  $V_n$  [26, 27, 28]. Appealing to interpolation between  $L^2(\Gamma)$  and  $H^1(\Gamma)$ , we conclude with

$$\|\mathbf{Q}_n u_{\Gamma}\|_{H^{\frac{1}{2}}(\Gamma)} \leq C \|u_{\Gamma}\|_{H^{\frac{1}{2}}(\Gamma)}, \quad (40)$$

which shows (38).

**Remark 2.** Summing up, the mesh-independent stability can be confirmed for DtN-based coupling from section 3.2 and for the multi-field approach from section 3.3, whereas it remains elusive for the least-squares technique examined in section 3.1. However, numerical tests, some of which are reported in the next section, do not confirm a superior performance of the two former approaches compared to the latter.

## 4. Numerical Experiments

Throughout we use piecewise linear Lagrangian finite elements, i.e.  $V_n = \mathcal{S}_1^0(\mathcal{M}_f)$  (see (37)), on triangular/tetrahedral meshes  $\mathcal{M}_f$  of  $\Omega_f$ .

To study the convergence we employ uniform  $h$ -refinement of  $\mathcal{M}_f$  and  $p$ -refinement of the Trefftz approximation, in the sense that we increase the number of multipole expansions. The  $p$ -refinement of the multipoles is carried out depending on  $h$ -refinement of  $\mathcal{M}_f$ . Details on this dependence are given for each convergence test.

We monitor the following  $L^2$ -errors:

1. The error in the FE domain, which is the relative  $L^2(\Omega_f)$ -error compared to the reference solution in  $\Omega_f$ , i.e.  $\|u - u_n\|_{L^2(\Omega_f)} / \|u\|_{L^2(\Omega_f)}$ ,  $u_n \in \mathcal{S}_1^0(\mathcal{M}_f)$  the finite element solution.
2. The MMP error on the interface, which is the relative  $L^2(\Gamma)$ -error compared to the reference solution on  $\Gamma$ .

The average between the relative  $L^2$ -error for FEM in  $\Omega_f$  and the relative  $L^2$ -error for MMP on  $\Gamma$  is the total relative error of the coupling.

To control the impact of numerical integration for FEM, we use a Gaussian quadrature rule that is exact for polynomials of degree 2 (order 3).

*Implementation.* The code is written in C++14, using C++11 multithreading for parallelization. We use Eigen v3.2.10 [29] for linear algebra and HyDi [30] for the FEM component. The PARDISO v5.0.0 solver [31, 32] provides the sparse LU decomposition to invert the matrices of the coupling, characterized by nontrivial sparsity patterns.

### 4.1. 2D Poisson's Equation With Exact Solution

We solve  $-\Delta u = j$  in  $\mathbb{R}^2$ , with piecewise constant source  $j$ ,  $|j| = 1.05 \cdot 10^6$  in  $\Omega_\star$  and  $= 0$  elsewhere.  $\Omega_\star$  is formed by two disks, with  $j$  having a different sign in each of them. The geometry is shown in fig. 4; the coupling boundary  $\Gamma$  is artificial.

The exact solution is given by the fundamental solution of 2D Poisson's equation integrated with Gaussian quadrature of order 3. Multipole expansions are uniformly positioned on a circle of radius 1 centered in the origin. We only use multipoles up to order 1.

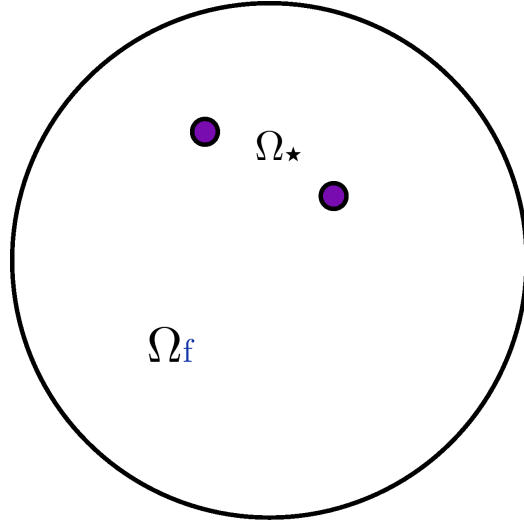


Figure 4: The geometry represents the FEM domain  $\Omega_f$ . The violet disks of radius 0.1 represent  $\Omega_*$ , the area where  $j$  is nonzero: in one it is  $= 1.05 \cdot 10^6$ , in the other  $= -1.05 \cdot 10^6$ . They are centered at  $(0.5, 0.5)^T$  and  $(-0.5, 1)^T$ . The black circle centered in the origin with radius 2 represents the artificial coupling boundary  $\Gamma$ .

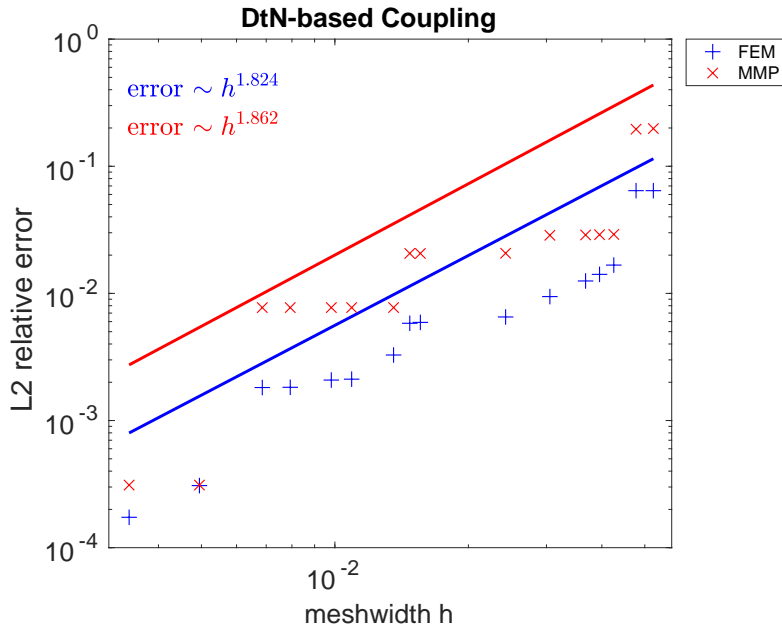


Figure 5:  $h$ -refinement log-log plot for 2D Poisson with exact solution. The number of multipoles is set to the logarithm of the number of vertices of the FEM meshes on  $\Gamma$ . Plot obtained with the DtN-based approach.

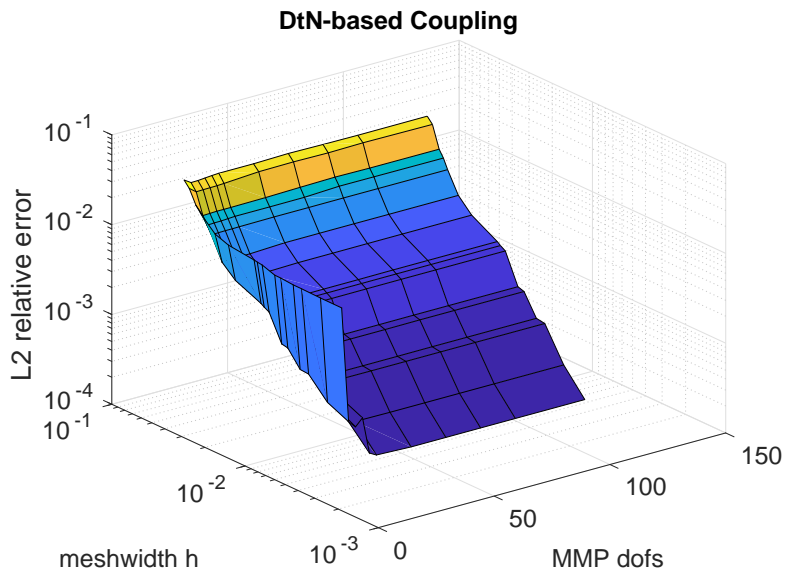


Figure 6: Meshwidth  $h$  vs. MMP degrees of freedom for 2D Poisson with exact solution: total relative error. The  $h$ - and error-dimensions are in logarithmic scale. Plot obtained with the DtN-based approach.

Figure 5 shows the  $h$ -refinement convergence plot for the DtN-based approach. In order to balance the errors, the number of multipoles is set to the natural logarithm of the number of vertices of the FEM meshes on the boundary  $\Gamma$ . This reflects the expected exponential convergence of the MMP approximation versus the algebraic convergence of the FE approximation.

Plots obtained with the other approaches look the same. We can clearly identify a quadratic convergence of the FEM and MMP errors in terms of the meshwidth.

Figure 6 shows a surface plot of the total relative  $L^2$ -error for the DtN-based approach. Plots obtained with the other approaches look the same. The error decreases with  $h$  (algebraic convergence) and is generally independent from the number of multipoles. This is due to the fact that the exact solution is so easy to approximate in the MMP domain that it can already be represented by very few multipoles. However, the error also becomes worse with the coarsest meshes and the highest number of multipoles considered: the FE error dominates.

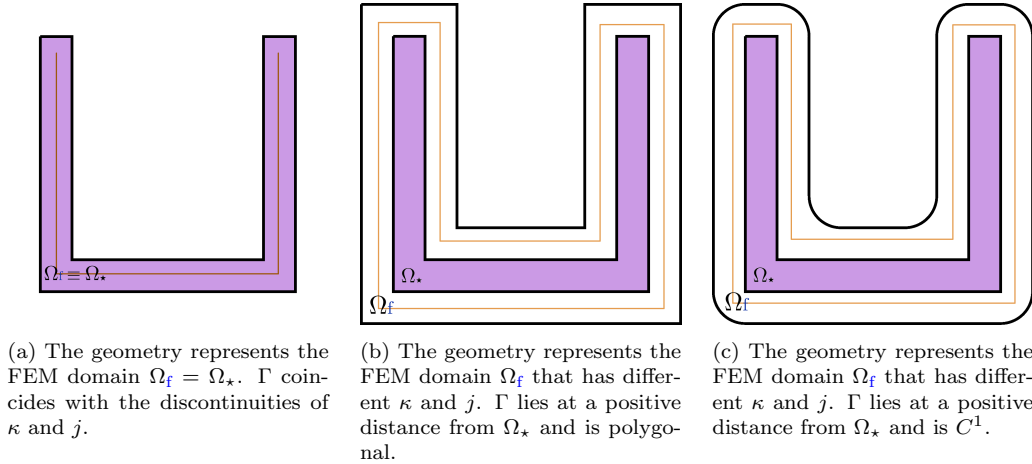


Figure 7: The **violet** U-shape, which fits into  $[-1, 1]^2$ , represents  $\Omega_*$  with  $\kappa = \frac{1}{10}$  and  $j = 1.05 \cdot 10^6$ . The other part of the geometry is characterized by  $\kappa = 1$  and  $j = 0$ . The **brown** line is the curve along which multipoles are positioned uniformly. Local refinement at the corners of the internal square (where the meshwidth  $h$  is  $\sim r^3$ , with  $r$  distance from the closest corner) is needed because the solution is not smooth there.

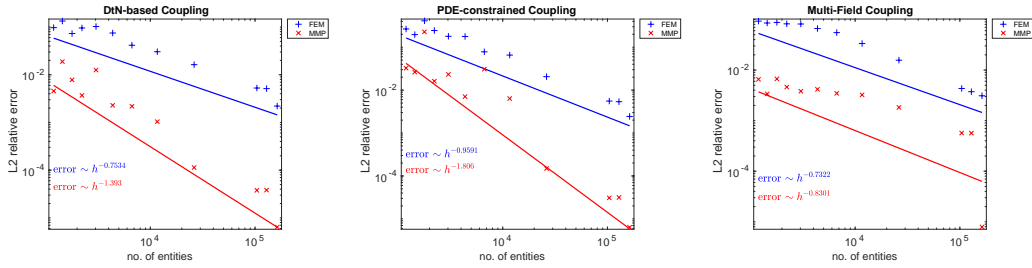
#### 4.2. 2D Diffusion Problem with Jumping Coefficients

We solve  $-\nabla \cdot (\kappa \nabla u) = j$  in  $\mathbb{R}^2$ , with  $\kappa = \frac{1}{10}$ ,  $j = 1.05 \cdot 10^6$  in  $\Omega_*$  and  $\kappa = 1$ ,  $j = 0$  elsewhere.  $\Omega_*$  is the U-shaped region displayed in fig. 7. For want of an exact solution, as reference solution we rely on the numerical solution provided by a mesh substantially more refined than the finest mesh used in the convergence study.

All types of meshes employed are shown in fig. 7: we consider three examples where the boundary  $\Gamma$  has different positions and shapes.

With  $\Gamma$  at the discontinuities of  $\kappa$  and  $j$ , multipoles are uniformly positioned along the skeleton inside  $\Omega_f$  (see fig. 7a). With  $\Gamma$  at a positive distance from  $\Omega_*$ , that is, in the case of an artificial coupling boundary, multipoles are uniformly positioned along a line following the skeleton of  $\Omega_f \setminus \Omega_*$ , which is positioned at a distance of 0.15 from  $\partial\Omega_*$  (see figs. 7b and 7c). We only use multipoles of order 0 (fundamental solutions of  $-\Delta u = 0$ ).

Given the different boundaries  $\Gamma$ , for a fair comparison the MMP error has not been computed as a boundary error, but on coarser meshes encompassing the area around  $\Omega_f$  bounded by  $[-4, 4]^2$ . The number of multipoles is set to the natural logarithm of the number of vertices of the FEM meshes on the boundary  $\Gamma$ , multiplied by 10.



(a) Obtained with the DtN- (b) Obtained with the PDE- (c) Obtained with the multi-field  
 based approach. constr. approach. approach.

Figure 8:  $h$ -refinement log-log plots for 2D Poisson without exact solution. Along the  $x$ -axis we show the number of entities of the FEM mesh. The number of multipoles is set to the logarithm of the number of vertices of the FEM meshes on  $\Gamma$ , multiplied by 10.  $\Gamma$  coincides with the discontinuities of  $\kappa$  and  $j$  (see fig. 7a).

Figure 8 shows the  $h$ -refinement convergence plots for all coupling approaches given  $\Gamma$  at the discontinuities. We can identify an algebraic convergence of the FEM and MMP errors, but with quite different rates depending on the coupling approach.

Figure 9 shows the  $h$ -refinement convergence plots for the DtN-based approach given  $\Gamma$  at a positive distance from  $\Omega_*$ , either with or without corners. Plots obtained with the other approaches look the same. We can clearly identify an algebraic convergence of the FEM and MMP errors.

#### 4.3. 3D Poisson's Equation With Exact Solution

We solve  $-\Delta u = q$  in  $\mathbb{R}^2$ , with  $q = \frac{3}{4\pi}$  in  $\Omega_*$  and  $= 0$  elsewhere.  $\Omega_*$  is formed by a sphere of radius 1 centered at  $(0, 0, 0.5)^\top$ . The geometry is shown in fig. 10; the coupling boundary  $\Gamma$  is artificial.

The exact solution is given by an exact integration inside  $\Omega_*$  and the fundamental solution of 3D Poisson's equation (integrated with Gaussian quadrature of order 3) outside. Multipole expansions are uniformly positioned on a circle of radius 1 centered in the origin and lying on the  $XY$ -plane. We only use multipoles up to order 1.

Figure 11 shows the  $h$ -refinement convergence plot for the DtN-based approach. The number of multipoles is set to the natural logarithm of the number of vertices of the FEM meshes on the boundary  $\Gamma$ . Plots obtained with the other approaches look the same. We can identify an algebraic convergence of the FEM and MMP errors.

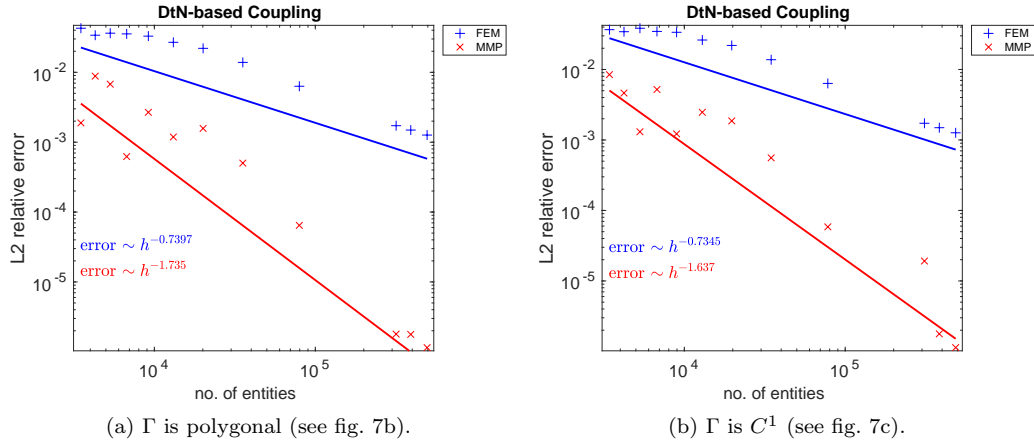


Figure 9:  $h$ -refinement log-log plots for 2D Poisson without exact solution. Along the  $x$ -axis we show the number of entities of the FEM mesh. The number of multipoles is set to the logarithm of the number of vertices of the FEM meshes on  $\Gamma$ , multiplied by 10.  $\Gamma$  lies at a positive distance from  $\Omega_*$ . Plots obtained with the DtN-based approach.

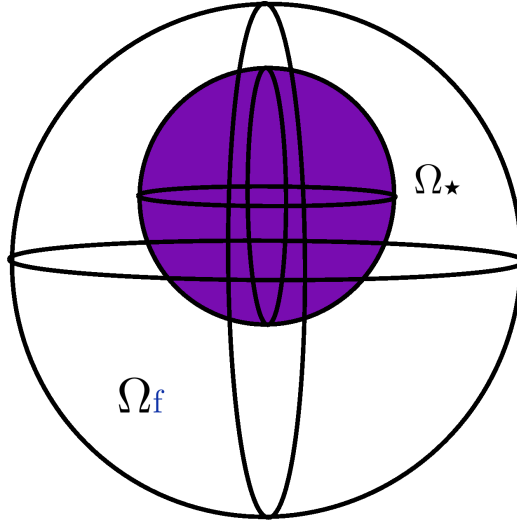


Figure 10: Cross-section of 3D geometry along the  $XZ$ -plane. The big sphere represents the FEM domain  $\Omega_f$ . The violet sphere of radius 1 represents  $\Omega_*$ , the volume where  $q \neq 0$ . It is centered at  $(0, 0, 0.5)^\top$ . The large sphere centered in the origin with radius 2 represents the artificial coupling boundary  $\Gamma$ .

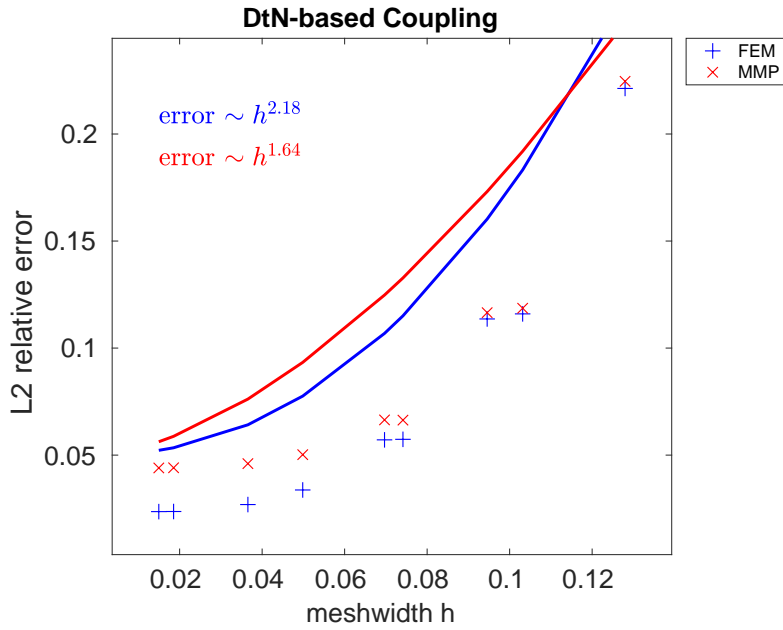


Figure 11:  $h$ -refinement plot for 3D Poisson with exact solution. The number of multipoles is set to the logarithm of the number of vertices of the FEM meshes on  $\Gamma$ . Plot obtained with the DtN-based approach.

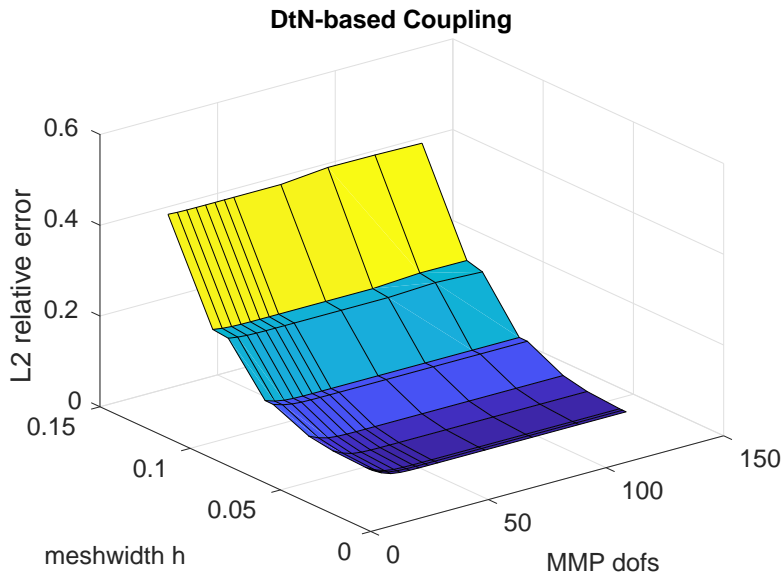


Figure 12: Meshwidth  $h$  vs. MMP degrees of freedom for 3D Poisson with exact solution: total relative error. Plot obtained with the DtN-based approach.



Figure 12 shows the surface plot of the total relative  $L^2$ -error for the DtN-based approach. Plots obtained with the other approaches look the same. The error decreases with  $h$  (algebraic convergence) and is generally independent from the number of multipoles.

## 5. Conclusions

Among the three coupling approaches presented in sections 3.1 to 3.3, none is clearly superior. We recommend the DtN-based approach thanks to its complete convergence theory and good practical performance. We point out that in this work several important issues have not been addressed: solving the linear systems (iteratively), ill-conditioning when using many or high-order multipoles, and vector Maxwell's equations.

## 6. Acknowledgements

This work was supported by the Swiss National Science Foundation [grant number 2000021\_165674/1].

## References

- [1] W. McLean, *Strongly Elliptic Systems and Boundary Integral Equations*, Cambridge University Press, 2000.
- [2] R. Hiptmair, A. Moiola, I. Perugia, *A Survey of Trefftz Methods for the Helmholtz Equation*, Springer, Cham, 2016, pp. 237–279. doi:10.1007/978-3-319-41640-3\_8.
- [3] C. Chen, S. Reutskiy, V. Rozov, The method of the fundamental solutions and its modifications for electromagnetic field problems, *Computer Assisted Methods in Engineering and Science* 16 (1) (2017) 21–33. URL <http://comes.ippt.gov.pl/index.php/comes/article/view/161>
- [4] T. Betcke, L. N. Trefethen, Reviving the Method of Particular Solutions, *SIAM Review* 47 (3) (2005) 469–491. doi:10.1137/S0036144503437336.

- [5] D. I. Kaklamani, H. T. Anastassiou, Aspects of the Method of Auxiliary Sources (MAS) in computational electromagnetics, *IEEE Antennas and Propagation Magazine* 44 (3) (2002) 48–64. doi:10.1109/MAP.2002.1028734.
- [6] Y.-S. Smyrlis, Applicability and Applications of the Method of Fundamental Solutions, *Mathematics of Computation* 78 (267) (2009) 1399–1434.  
URL <http://www.jstor.org/stable/40234665>
- [7] M. Katsurada, Charge simulation method using exterior mapping functions, *Japan Journal of Industrial and Applied Mathematics* 11 (1) (1994) 47. doi:10.1007/BF03167213.
- [8] M. Katsurada, H. Okamoto, The collocation points of the fundamental solution method for the potential problem, *Computers & Mathematics with Applications* 31 (1) (1996) 123–137. doi:https://doi.org/10.1016/0898-1221(95)00186-3.
- [9] K. Sakakibara, Analysis of the dipole simulation method for two-dimensional Dirichlet problems in Jordan regions with analytic boundaries, *BIT Numerical Mathematics* 56 (4) (2016) 1369–1400. doi:10.1007/s10543-016-0605-1.
- [10] Y. A. Eremin, A. G. Sveshnikov, A Computer Technology for the Discrete Source Method in Scattering Problems, *Computational Mathematics and Modeling* 14 (1) (2003) 16–25. doi:10.1023/A:1022069632726.
- [11] C. J. Gittelsohn, R. Hiptmair, I. Perugia, Plane wave discontinuous Galerkin methods: Analysis of the  $h$ -version, *ESAIM: Mathematical Modelling and Numerical Analysis* 43 (2) (2009) 297–331. doi:10.1051/m2an/2009002.
- [12] R. Hiptmair, A. Moiola, I. Perugia, Plane wave discontinuous Galerkin methods for the 2D Helmholtz equation: Analysis of the  $p$ -version, *SIAM Journal on Numerical Analysis* 49 (1) (2011) 264–284. doi:10.1137/090761057.
- [13] R. Hiptmair, A. Moiola, I. Perugia, Stability results for the time-harmonic Maxwell equations with impedance boundary conditions,

Mathematical Models and Methods in Applied Sciences 21 (11) (2011) 2263–2287. doi:10.1142/S021820251100574X.

- [14] R. Hiptmair, A. Moiola, I. Perugia, Plane Wave Discontinuous Galerkin Methods: Exponential Convergence of the *hp*-Version, Foundations of Computational Mathematics 16 (3) (2016) 637–675. doi:10.1007/s10208-015-9260-1.
- [15] R. Hiptmair, A. Moiola, I. Perugia, Error analysis of Trefftz-discontinuous Galerkin methods for the time-harmonic Maxwell equations, Mathematics of Computation 82 (281) (2013) 247–268. doi:10.1090/S0025-5718-2012-02627-5.
- [16] A. Barnett, T. Betcke, Stability and convergence of the method of fundamental solutions for Helmholtz problems on analytic domains, Journal of Computational Physics 227 (14) (2008) 7003–7026. doi:https://doi.org/10.1016/j.jcp.2008.04.008.
- [17] A. H. Barnett, T. Betcke, An Exponentially Convergent Nonpolynomial Finite Element Method for Time-Harmonic Scattering from Polygons, SIAM Journal on Scientific Computing 32 (3) (2010) 1417–1441. doi:10.1137/090768667.
- [18] P. R. S. Antunes, A numerical algorithm to reduce ill-conditioning in meshless methods for the Helmholtz equation, Numerical Algorithms 79 (3) (2018) 879–897. doi:10.1007/s11075-017-0465-z.
- [19] J. Smajic, C. Hafner, J. Leuthold, Coupled FEM–MMP for Computational Electromagnetics, IEEE Transactions on Magnetics 52 (3) (2016) 1–4. doi:10.1109/TMAG.2015.2475241.
- [20] C. Hafner, Beiträge zur Berechnung der Ausbreitung elektromagnetischer Wellen in zylindrischen Strukturen mit Hilfe des “Point-Matching”-Verfahrens, Dissertation 6683, ETH Zurich, Switzerland (1980).
- [21] G. Mie, Elektrische Wellen an zwei parallelen Drähten, Annalen der Physik 307 (1900) 201–249. doi:10.1002/andp.19003070602.
- [22] I. N. Vekua, New methods for solving elliptic equations, North Holland Publishing Company, 1967.

- [23] A. Moiola, Trefftz-Discontinuous Galerkin Methods for Time-Harmonic Wave Problems, Dissertation 19957, Seminar for Applied Mathematics, ETH Zurich, Switzerland (2011). doi:10.3929/ethz-a-006698757.
- [24] P. Monk, Finite Element Methods for Maxwell's Equations, Clarendon Press, 2003.
- [25] D. Braess, Finite Elements: Theory, Fast Solvers, and Applications in Solid Mechanics, 3rd Edition, Cambridge University Press, 2007. doi:10.1017/CB09780511618635.
- [26] J. H. Bramble, J. E. Pasciak, O. Steinbach, On the Stability of the  $L^2$  Projection in  $H^1(\Omega)$ , Mathematics of Computation 71 (237) (2002) 147–156.  
URL <http://www.jstor.org/stable/2698864>
- [27] R. E. Bank, H. Yserentant, On the  $H^1$ -stability of the  $L^2$ -projection onto finite element spaces, Numerische Mathematik 126 (2) (2014) 361–381. doi:10.1007/s00211-013-0562-4.
- [28] C. Carstensen, Merging the Bramble-Pasciak-Steinbach and the Crouzeix-Thomé Criterion for  $H^1$ -Stability of the  $L^2$ -Projection onto Finite Element Spaces, Mathematics of Computation 71 (237) (2002) 157–163.  
URL <http://www.jstor.org/stable/2698865>
- [29] G. Guennebaud, B. Jacob, Eigen v3.3.4, <http://eigen.tuxfamily.org> (2017).
- [30] R. Casagrande, C. Winkelmann, Hybrid Discontinuous Finite Elements for Power Devices, ABB Corporate Research Center (2016).
- [31] C. G. Petra, O. Schenk, M. Lubin, K. Gärtner, An augmented incomplete factorization approach for computing the Schur complement in stochastic optimization, SIAM Journal on Scientific Computing 36 (2) (2014) C139–C162.
- [32] C. G. Petra, O. Schenk, M. Anitescu, Real-time stochastic optimization of complex energy systems on high-performance computers, IEEE Computing in Science & Engineering 16 (5) (2014) 32–42.